Radio Science, Volume 36, Number 4, Pages 671–680, July–August 2001

Using geomagnetic birefringence to locate sources of impulsive, terrestrial VHF signals detected by satellites on orbit

Abram R. Jacobson and Xuan-Min Shao

Space and Atmospheric Sciences Group, Los Alamos National Laboratory, Los Alamos, New Mexico

Abstract. The Earth's ionosphere is magnetized by the geomagnetic field and imposes birefringent modulation on VHF radio signals propagating through the ionosphere. Satellites viewing VHF emissions from terrestrial sources receive ordinary and extraordinary modes successively from each broadband pulse emitted by the source. The birefringent intermode frequency separation can be used to determine the value of f_{ce} cos β, where f_{ce} is the electron gyrofrequency and β is the angle between the wave vector **k** and the geomagnetic field **B** at the point where the VHF ray path intersects the ionosphere. Successive receptions of multiple signals (from the same source) cause variation in f_{ce} cos β, and from the resulting variation in the signal intermode frequency separation the source location on Earth can be inferred. We test the method with signals emitted by the Los Alamos Portable Pulser and received by the FORTE satellite.

1. Introduction

This article proposes a new method for determining the location on Earth of impulsive radio emissions, by exploiting the characteristics of signals acquired by radio receivers aboard Earth-orbiting satellites. The new method is not related either to interferometric direction finding or to time-of-arrival (TOA) methods. Instead, the new method takes advantage of the signal modulation imposed by the radio frequency birefringence of the Earth's ionosphere.

Satellites are the only platform for global collection of very high frequency (VHF; 30–300 MHz) radiation, which is not ducted over the horizon by the ionosphere. VHF emanations from sources beyond the horizon cannot be monitored by ground-based sensors. A single satellite fares poorly at determining the latitude and longitude (geolocation) of a source in the low VHF. The satellite antenna lobe angular width is approximately λ/D (radians), where λ is the radio wavelength and D is the antenna aperture. At 30 MHz (λ = 10 m), even a deployed 10-m antenna would have a beam of ~1-rad width, which is quite poor for geolocation. For a low-Earth-orbit (LEO) satellite to achieve even crude 100-km resolution at nadir from 1000-km altitude, an extremely expensive 100-m deployed antenna would be required. The alternative is to fly a satellite constellation, with at least three satellites required to geolocate the source by TOA techniques. In either case, geolocation resolution drives the mission cost to escalate nonlinearly.

Many radio frequency signals, such as those emanating from lightning storms, occur repetitively during the passage of a LEO satellite within view of the source or source cluster. During such a series of signal repetitions from the same location, the LEO satellite (~100-min orbital period) moves relative to the source. The RF line of sight at each instant in the orbit passes from the source, through the Earth's ionosphere, to the satellite. The RF signal is dispersed in the ionospheric plasma, and the dispersed signal is further separated into "magnetoionic" modes [*Budden*, 1988] of radio propagation due to the plasma's birefringence. To first approximation, the instantaneous frequency separation of the two modes (at any given time in the received waveform) is $2f_{ce}$ cos β, where f_{ce} is the electron-cyclotron frequency, proportional to magnetic field (2.80 MHz G^{-1}), and β is the angle between the field **B** and the RF wave vector **k**. This forms the basis for cumulative inference of the source location: As the satellite receives subsequent repetitions of signal from the same source but with the receiver at different orbital positions, the observable intermode frequency separation $2f_{ce}$ cos β changes in a predictable way that

Paper number 2000RS002555.
0048-6604/01/2000RS002555$11.00

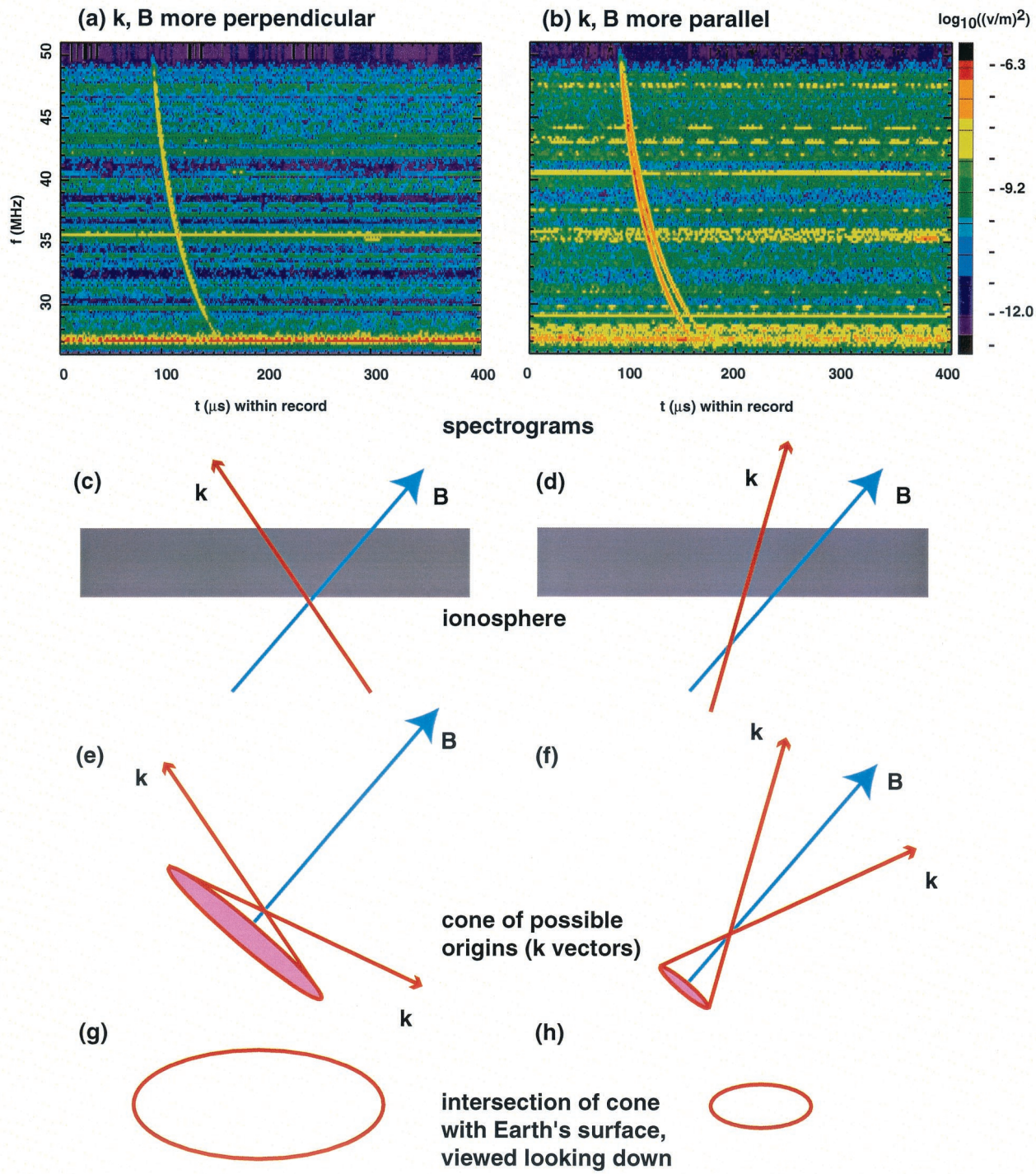

Plate 1. Comparison of birefrigence-based location constraints for **k** and **B** more perpendicular (left column) and **k** and **B** more parallel (right column). (a and b) Spectrograms of Los Alamos Portable Pulser (LAPP) impulses received by FORTE. The overall f^{-2} dispersion is due to ionospheric plasma. The intermode frequency separation (see Plate 1a) is due to geomagnetic birefringence. (c and d) Angular relation to **k** and **B** within ionosphere. (e and f) Cones of possible arrival directions based on geomagnetic constraint. (g and h) Intersection of those cones with the Earth's surface.

depends on source and satellite locations. The latter is known, and the former can be uniquely retrieved.

2. Concept

The ionospheric plasma disperses a radio pulse as it propagates from the ground to a satellite. Consider an impulsive, broadband radio emission from a location on the surface, or near the surface, of the Earth. The pulse essentially fills the frequency bandwidth of the radio receiver. In the absence of geomagnetic birefringence the index of refraction would be approximately [*Budden*, 1988] given by

$$\mu \approx 1 - \frac{1}{2}\frac{f_p^2}{f^2}, \tag{1}$$

where f_p is the plasma frequency and f is the radio frequency. Here we have assumed that $f_p^2 \ll f^2$, as is readily the case in this work, where the effective passband employed by the FORTE receivers is f = 26–48 MHz, while typically the plasma frequency is in the range 3–8 MHz. The group delay for propagation is

$$\tau = \frac{1}{2\pi}\int \frac{dk}{df}\,ds, \tag{2}$$

where k is the wave number and ds is the path element along the propagation path. From (1) and (2) we obtain

$$\tau = \frac{R}{c} + \frac{1}{2c}\int \frac{f_p^2}{f^2}\,ds = \frac{R}{c} + \frac{\alpha N}{f^2}. \tag{3}$$

Here, R is the straight path distance from the source to the satellite, c is the speed of light in vacuum, N (in m^{-2}) is the slant total electron content along the straight path, α is 1.34×10^{-7}, and f is the frequency (in hertz). We may invert (3) to express the frequency as a function of time during the dispersed "chirp" received at the satellite:

$$f = \sqrt{\frac{\alpha N}{t - t_0}}, \tag{4}$$

where t_0 is the time of arrival in lieu of ionospheric dispersion. Equation (4) shows the increasingly delayed arrival time as the frequency is reduced. Put another way, the higher frequencies in the passband arrive earlier, and the lower frequencies arrive later.

This analysis can be extended to include the effect of the Earth's dipole magnetic field. This field varies (in magnitude and direction) gradually versus position, on a spatial scale comparable to the Earth's radius, while the ionospheric F layer (where most ionospheric density resides) is only ~100–200 km thick, or a few percent of the Earth's radius. The birefringence is generated only where there is significant plasma density, that is, within the relatively thin shell (on the scale of the magnetic field variations) represented by the F layer. That is why we are justified in treating the birefringence as if the ionosphere were a thin layer, of path-integrated density N, located at the altitude of the F layer, and as if the birefringence occurred for the value of the vector magnetic field where the radio propagation path (line of sight) pierces that layer. Performing this analysis [*Massey et al*., 1998], we find that the dispersive arrival of frequencies is described by

$$f = \sqrt{\frac{\alpha N}{t - t_0}} \pm f_{ce}\cos\beta, \tag{5}$$

where f_{ce} is the electron gyrofrequency (in hertz) and β is the angle between the wave vector **k** and the geomagnetic field **B**, at the point where the line of sight pierces the F layer. The minus sign is for the ordinary mode, while the plus sign is for the extraordinary mode [*Budden*, 1988]. In practice, the ionospheric F layer dominates the accumulated refractivity, so the appropriate value of $f_{ce}\cos\beta$ in (5) is that near the peak of the F layer.

Equation (5) is derived under the "quasilongitudinal approximation," which is valid only where $|\cos\beta/\sin^2\beta| \gg f_{ce}/(2f)$ [*Budden*, 1988]. If we take f_{ce} = 0.3 MHz and f = 30 MHz, then we require $|\beta - 90°| \gg 0.3°$. That is, the approximation breaks down only within a degree of **k** and **B** being exactly orthogonal. Thus the quasilongitudinal approximation is robustly satisfied for essentially all of our data.

The effect of birefringence can be described as the simultaneous arrival of energy at frequencies $f \pm f_{ce}\cos\beta$. At any given time, energy at the frequency $f + f_{ce}\cos\beta$ is from the extraordinary mode, while energy at the frequency $f - f_{ce}\cos\beta$ is from the ordinary mode. (In the absence of the geomagnetic field the energy that would would be arriving at this time would have the single frequency f.) Provided that the source is linearly polarized, a particularly efficient way of extracting $f_{ce}\cos\beta$ is to measure the beat frequency between the extraordinary and ordinary modes. For unpolarized sources the methods of ex-

tracting f_{ce} cos β are slightly more cumbersome but are nonetheless straightforward.

The key concept in this proposal is that measurement from one satellite location of $\delta f = 2f_{ce}$ cos β constrains the possible locations of the source on Earth. Plate 1 shows the situation for two possible orientations of the **k** vector with respect to the same **B** vector: In the left column, **k** is less parallel to **B**; that is, the angle β is closer to 90°. In the right column, **k** is more parallel to **B**; that is, the angle β is closer to 0°. The spectrograms in Plates 1a and 1b are real data from the FORTE satellite [*Jacobson et al.*, 1999] illuminated by the Los Alamos Portable Pulser (LAPP), a broadband, high-power VHF impulsive source [*Massey et al.*, 1998]. In each case, as in all data to be used in this study, the passband is effectively 26–48 MHz (although the full Nyquist passband extends to 53 MHz). The spectrogram in Plate 1a shows less mode separation. The spectrogram in Plate 1b shows more mode separation. Plates 1c and 1d show sketches of the ionospheric interaction region, where the intermode frequency separation occurs. Plates 1e and 1f show sketches of the cones of possible **k** vectors consistent with the measured values of $\delta f = 2f_{ce}$ cos β. Plates 1g and 1h show sketches of those cones' intersections with the Earth's surface. The source is inferred to lie on such a curve of intersection.

Next, how can these constraints be combined to yield a point geolocation? This is done by combining data from at least three repeated emissions, from separated satellite positions. Figure 1 is a sketch of the collection of three separate VHF signals from the same source on Earth. Each signal propagates through the ionosphere's principal layer, where it makes an angle β with the geomagnetic field **B**.

For each position of the satellite the received signal's intermode frequency separation tags the pertinent value of f_{ce} cos β, indicating a cone on which the source must lie. Each cone's intersection with the Earth's surface is a closed curve and is shown in sketch form in Figure 2. The source location is inferred to be at the intersection of the three closed curves. (In this respect the present geomagnetic approach to inferring location gives a graphical end product that is analogous to the isochrones of TOA.) The only possibility of twofold ambiguity would occur if the satellite orbital plane coincided with a magnetic meridian plane; however, such a case would be rare.

A remarkable feature of the present approach to geolocation is that the cone-intersection curves can be amassed cumulatively over time, each curve being stored in an archive which would be periodically opened and searched for common intersections. The detailed waveforms do not have to be the same between repeated receptions; they just have to possess enough bandwidth to enable retrieval of $\delta f = 2f_{ce}$ cos β. This is a fundamental advantage over TOA, allowing attribution to be inferred a posteriori from a cumulative archive of closed curves on a map of the Earth's surface.

3. Test of the Geolocation Concept

The FORTE satellite has collected impulsive signal waveforms from the LAPP on more than 1000 occasions [*Jacobson et al.*, 1999]. The data used here will be those FORTE signals from LAPP illuminations in which the data were acquired by the 50-megasample-per-second receiver set to cover the range 26–51 MHz, i.e., the FORTE "low band" [*Jacobson et al.*, 1999].

For each LAPP signal in this low band we analyze 40 μs of data centered on the arrival time of the pulse. Equation (5) shows that if we square the signal, the square will manifest an amplitude modulation at beat frequency $\delta f = 2f_{ce}$ cos β, due to the interference between the extraordinary and ordinary modes. To exploit the beating for retrieval of f_{ce} cos β, after squaring the signal we smooth the squared signal by averaging within a sliding 0.2-μs window, then take the power spectrum of the smoothed squared signal. The peak in the power spectrum, provided there is a significant peak, will reveal the parameter $\delta f = 2f_{ce}$ cos β.

Figure 3 shows this for one event. The bottom panel shows the smoothed square of the signal, while the top panel shows the power spectrum of the smoothed square of the signal. The smoothed square of the signal is modulated, almost fully, at a frequency of ~1.9 MHz. The peak at 0 MHz in the power spectrum is related to the overall offset and can be ignored; the modulation causes the second peak at 1.9 MHz. Evidently, then, the parameter f_{ce} cos β is approximately 0.95 MHz.

The quality of the fading spectral peak (see top panel of Figure 3) varies somewhat among the FORTE recordings of LAPP signals. We have chosen simply to select the peak of the spectrum as the indicator of $2f_{ce}$ cos β, but we do not mean to imply that this choice is necessarily better than using a power-weighted determination of the spectral peak.

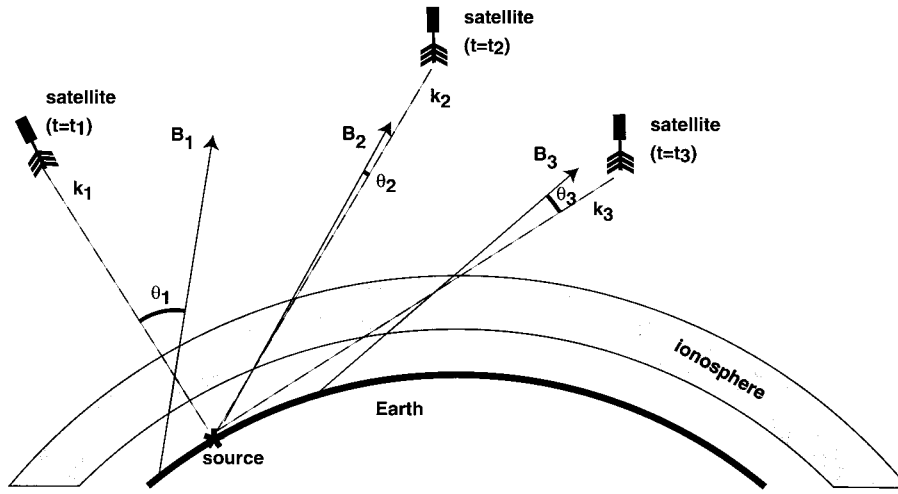

Figure 1. Relationship of **k** and **B** within ionosphere for three successive satellite receptions of signal from the same source.

The fact that the peak has some measurable width is not predicted by the simplified arguments leading to (5) and must indicate some inaccuracies in our approximate model. In general, our experience with LAPP signals recorded by FORTE indicates that the intrinsic uncertainty in the measurement of $2f_{ce}$ cos β, as indicated by the spectral width of the fading peak, is at least 0.03 MHz (best case) and frequently deteriorates to 0.15 MHz. We surmise that the failure of the peak to be a perfectly narrow spike (on the frequency axis), as would be suggested by our simplified model, is due to (1) finite signal-to-noise ratio, (2) imprecision of the thin-shell ionosphere model, (3) imprecision of the quasi-longitudinal approximation, and (4) higher-order (i.e., quartic) effects in the basic ionospheric dispersion as a function of $1/f$.

To analyze the entire set of FORTE low-band LAPP signal collections, we impose a signal-to-noise requirement on the power spectrum (see top panel in Figure 3): We require that the secondary peak in the frequency range 0.3–3.0 MHz exceed the median level in that frequency range by a factor of at least 20. This results in a set of only 628 acceptable low-band LAPP signals contributing to what follows. (The rest of the LAPP signals did not achieve this signal-to-noise ratio in their amplitude modulation.)

These 628 LAPP signals were intermittently gathered by FORTE over a campaign covering more than

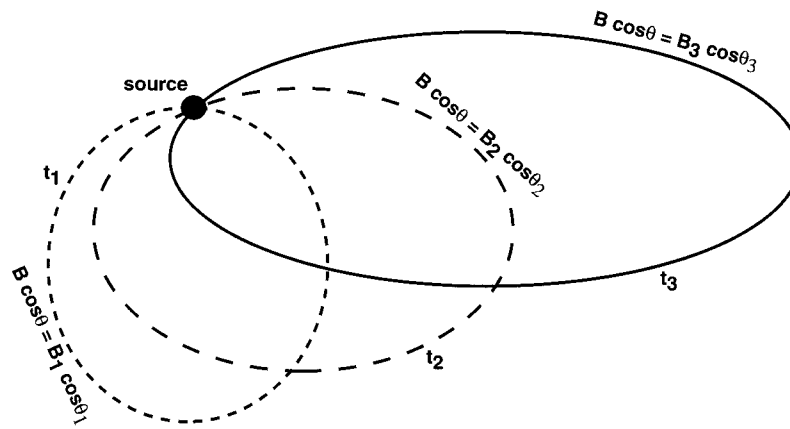

Figure 2. Closed curves of source location constraints (on surface of the Earth) for the three lines of sight shown in Figure 1. Note the unique intersection corresponding to the source location.

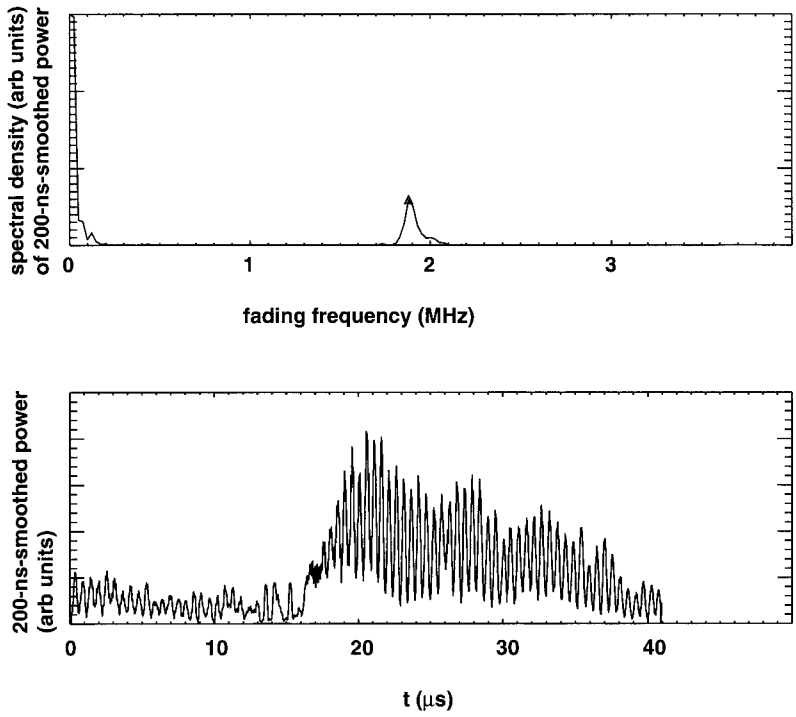

Figure 3. Amplitude-modulated power data from a single LAPP impulse received by FORTE's 26–51-MHz passband receiver (file f19981221_234108, event 727, channel a). (top) Power spectrum of 200-ns-averaged power. (bottom) Power averaged in sliding, 200-ns window.

a year. Most of the collections were during daylight, but the season, solar activity, and geomagnetic storm conditions varied widely. Therefore we do not expect the ionospheric effective altitude to have been perfectly constant during the collection of all our data; it may have varied over the range 250–500 km during this campaign. Nonetheless, this variability in expected effective altitude remains small compared to the spatial scale (the Earth's radius) over which **B** varies, so we are somewhat justified in comparing our data to a standard altitude ionosphere model. However, we must bear in mind that this model is only approximate, as is, for that matter, the assumption that we may treat the ionosphere as a thin shell.

Plate 2 shows a map of the subsatellite location (longitude and latitude) for these 628 acceptable signal recordings of LAPP impulses. The top panel encodes the retrieved value of f_{ce} cos β as the color of the data point, ranging from 0.2 to 1.5 MHz (see color bar of top panel). The warmer-colored (yellow and amber) data points have lines of sight to the LAPP (which is at 35.87°N, −106.33°E) that are optimally aligned with **B** in the ionospheric *F* layer, resulting in the highest values of f_{ce} cos β for this data set. The coldest-colored (blue) data points are for lines of sight to the LAPP that are closer to being normal to **B** within the ionospheric *F* layer. It is this position-dependent heterogeneity of retrieved values of f_{ce} cos β that allows an inference of the source location.

The bottom panel of Plate 2 encodes the absolute value of the difference between measured (see top panel) and modeled f_{ce} cos β for this data set. The model is the International Geomagnetic Reference Field (IGRF) [*Barton*, 1997] updated to 1995. This model is appropriate below the magnetosphere. In our use of the IGRF we choose 400 km above the Earth as the effective height at which to evaluate f_{ce} cos β. This is an approximation of the entire ionospheric propagation as being equivalent to a penetration of one effective annular layer at 400 km. We have also varied the assumed height and found the results to be only weakly affected for the height within a range 250–500 km. A more precise approach would be to evaluate an integral of the refraction over a range of ionospheric heights. However, it will turn out (see equations (6)–(10)) that our errors are dominated

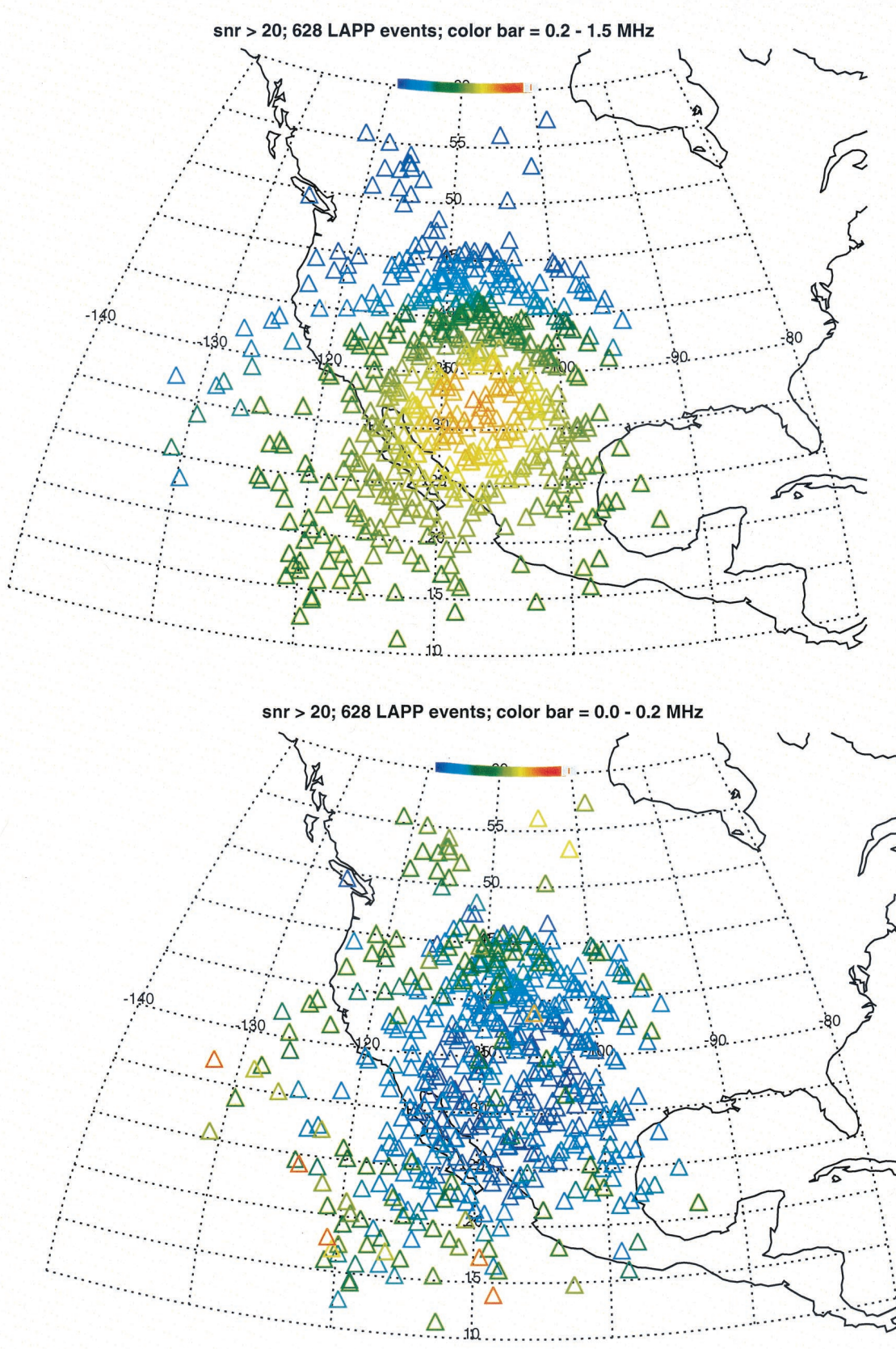

Plate 2. Map of subsatellite points during 628 accepted LAPP impulse receptions. (top) Color coding of inferred f_{ce} cos β from the pulse birefringence. (bottom) Magnitude of measured f_{ce} cos β minus modeled f_{ce} cos β, assuming a 400-km effective ionospheric layer height.

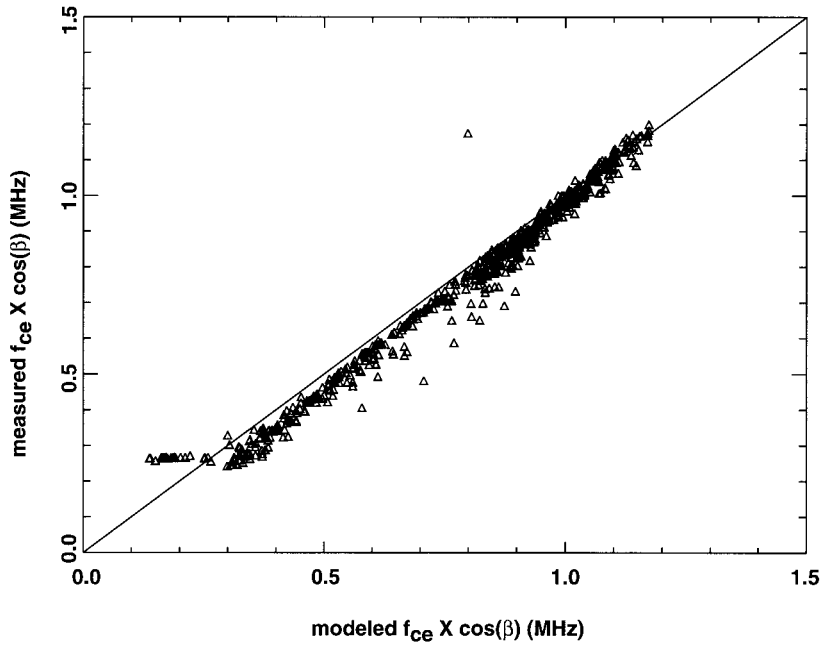

Figure 4. Measured f_{ce} cos β (vertical axis) versus modeled f_{ce} cos β (horizontal axis), assuming a 400-km effective ionospheric layer height. Here, snr $>$ 20; 628 LAPP events.

not by the thin-ionosphere assumption but rather by ray bending.

The bottom panel of Plate 2 shows that the discrepancies between the measurements and the model of f_{ce} cos β tend to be small in magnitude ($<$0.05 MHz) for high-elevation-angle lines of sight and/or for cos β near unity and tend to be larger in magnitude (up to or occasionally exceeding 0.1 MHz) for low-elevation-angle lines of sight and/or low values of cos β. This basic feature does not change if we vary the assumed ionospheric altitude (for evaluation of f_{ce} cos β in the model) within a reasonable range (250–500 km).

A way to gain better insight into the data/model discrepancies is to graph the measured versus the model results, as is done in Figure 4. The solid line indicates equality. Evidently, the discrepancies are least for large values of f_{ce} cos β, i.e., for close alignment of **k** and **B**. Similarly, the errors are larger for smaller values of f_{ce} cos β, i.e., for near-orthogonality of **k** and **B**. Note also that the errors tend to be of one sign: The measured f_{ce} cos β tends to be smaller than the modeled f_{ce} cos β, with the exceptions of one outlier and several points at the lowermost values of modeled f_{ce} cos β.

What distinguishes the majority of the data (for which the measured f_{ce} cos β is below the model values) from the several points at the far left (for which the measured f_{ce} cos β is above the model values? It turns out that there is a simple discriminant, tending to implicate ray bending as the dominant source of these measurements/model discrepancies. Figure 5 shows a sketch of ray bending. Since the radio frequency phase index of refraction is less than unity, a ray incident from the emitter (e) tends by Snell's Law to be bent into a more grazing angle (thick segment of ray path) through the ionosphere. Also shown in Figure 5 is the geomagnetic field direction (dashed line) evaluated at the ionospheric ray transit. Evidently, the effect of ray bending in the case shown here will be to increase the angle β between **k** and **B**, i.e., to reduce the measured f_{ce} cos β below the model value calculated as if ray bending did not occur. Moreover, the sensitivity of measured f_{ce} cos β to ray bending maximizes for β close to 90°.

It so happens that each of the data points in Figure 4 (see above) for which the measured f_{ce} cos β is below the model value also has a nominal ray path lower in elevation angle than **B**, as shown in Figure 5. Thus, for those majority events the increasing discrepancy between measured and modeled f_{ce} cos β (as cos β is reduced) is precisely what we would expect on the basis of the effect of ray bending.

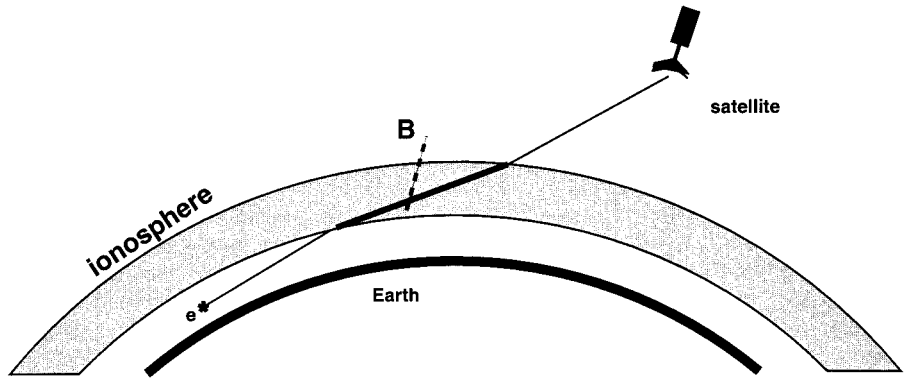

Figure 5. Sketch of ionospheric ray bending, for the majority case in which the effect of ray bending is to widen the angular separation between **k** and **B** within the ionosphere.

Moreover, the several points on the far left of Figure 4, for which the measured f_{ce} cos β is above the model value, all turn out to have the opposite arrangement of **B** and **k**; that is, the effect of ray bending is to increase f_{ce} cos β above the model value. The clear implication is that ionospheric ray bending might be producing the dominant error in the retrievals of f_{ce} cos β. (We cannot explain the single outlier point by this argument.)

The argument so far has shown that ray bending is consistent with the trends in Figure 4. In order to make credible the role of ray bending in producing the actual residuals shown by Figure 4 we need also to show that the expected ray bending order of magnitude at least suffices to generate the order-of-magnitude residual effects we see. What matters is the deviation of the ray path from the nominal line-of-sight direction, within the *F* layer. Snell's law provides that

$$u \sin \theta_{\text{ext}} = \sin\theta_{\text{int}} \tag{6}$$

is the relation of the incidence angle (off of normal) both external and internal to the ionosphere. Hence the ray bending internal to the ionosphere, relative to the nominal line of sight, is given by

$$\delta\theta = (\mu - 1) \tan \theta_1, \tag{7}$$

where θ_1 is unperturbed incidence angle. With reference to the situation in Figure 5, let us suppose that the plasma frequency in the ionosphere is $f_p = 5$ MHz. Then the index of refraction in the plasma (see equation (1)) for a radio frequency of 30 MHz will be $\mu = 1 - 0.014 = 0.986$. Thus, in this example, the refractive angular deviation (in radians) in the ionosphere will be $\delta\theta = 0.014 \tan \theta_1$.

On the other hand, the residual in f_{ce} cos β due to ray bending through an angle $\delta\beta$ will be

$$\delta(f_{ce} \cos \beta) = -f_{ce}\delta\beta \sin \beta. \tag{8}$$

Thus the fractional variation in f_{ce} cos β due to ray bending through an angle $\delta\beta$ will be

$$\frac{\delta(f_{ce} \cos \beta)}{(f_{ce} \cos \beta)} = -\delta\beta \tan \beta. \tag{9}$$

Noting that the largest value of $\delta\beta$ will be $\delta\theta$, we can substitute (7) into (9) to get

$$\frac{\delta(f_{ce} \cos \beta)}{(f_{ce} \cos \beta)} \leq (1 - \mu) \tan \beta \tan \theta_1 \tag{10}$$

in terms of magnitudes.

Inspecting Figure 4, we see that the fractional residual in the lower quarter of the plot is in the range 0.1–0.2. Noting that $1 - \mu = 0.014$, we see that (10) requires that tan β tan θ_1 be on the order of 10 for this to be satisfied. This is very easy to do with reasonable parameters, for example, if both β and θ_1 were 72°. Thus we conclude that refractive ray bending is not only implicated by the trend in the systematic residuals of Figure 4 but also easily capable of generating the required magnitudes of angular deviation.

4. Test for Accuracy of Geolocation

The data from these 628 events can be used to examine the possible accuracy of source geolocation through this novel geomagnetic method. To do this, we limit our attention to those lines of sight higher than 30° in elevation (seen from the source), so that

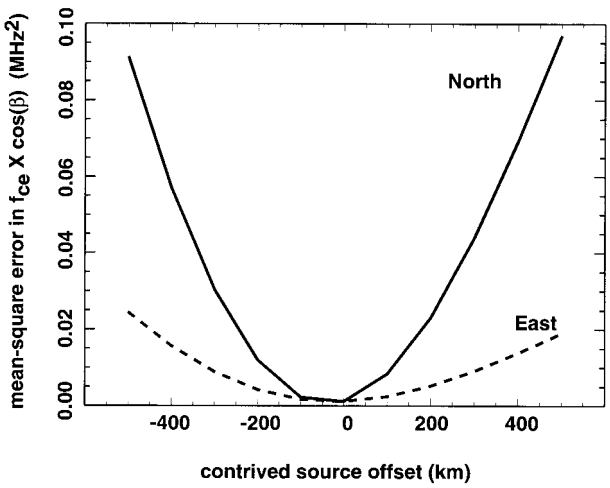

Figure 6. Response of mean-square residuals (in f_{ce} cos β) for north-south (solid curve) and east-west (dashed curve) contrived errors in source location. Elevation angle is greater than 30°.

we somewhat reduce the effects of ray bending. This still, it turns out, provides enough data "leverage" to allow successful, and rather accurate, geolocation, albeit still affected by ray bending.

To test the geolocation, we introduce an array of contrived source position errors, first a set of north-south errors and then a set of east-west errors, in 100-km steps out to ±500 km in both cases. Figure 6 shows the mean-square residuals for each such scan. The measurements of f_{ce} cos β do not change, but the model results of f_{ce} cos β do change, as a result of our inserting the contrived source location errors. The curves of square residuals clearly minimize within a few tens of kilometers of the true source position, and the curvature of the square residuals about their minima indicates that the positional resolution is less than 50 km north-south, and perhaps 100 km east-west. Moreover, the north-south square residuals are minimized by placement of the source 30–40 km north of the true source location. This can be shown to be a systematic effect of ray bending, especially of the lines of sight to the north of the LAPP but within the 30° elevation angle acceptance cone.

5. Conclusions

The new method of geolocation presented here is based on measurement of f_{ce} cos β via the complex signal modulation imposed on broadband VHF signals as they transit the ionosphere. The method is limited to signals in the low VHF, because the birefringent intermode frequency separation varies as f^{-3}, and higher frequencies would lack sufficient sensitivity. Moreover, the method is limited to repetitive signals which can be viewed by a satellite at several positions in the satellite orbit. One example of broadband signals which can be viewed repetitively by a satellite at several orbital positions is the VHF signatures of lightning. There may be anthropogenic radio emitters locatable in this manner as well.

We have tested the method using a data set based on anthropogenic broadband radio emissions from the Los Alamos Portable Pulser at 35.87°N, −106.33°E. Analysis of the data set indicates that the primary source of error in this method of geolocation is likely to be ionospheric ray bending. Analysis also indicates that positional accuracies of tens of kilometers (on the Earth's surface) may be expected for reasonably high-quality data. This is adequate, for example, to allow association of VHF lightning signatures with specific storm system features in geostationary satellite visible and infrared imagery.

Acknowledgments. The work described here was performed under the auspices of the U.S. Department of Energy. We are indebted to the FORTE operations team, led by Phil Klingner and Diane Roussel-Dupré, for constant support in acquiring and working with FORTE data. We are also indebted to David Smith and Daniel Holden for operation of the LAPP facility.

References

Barton, C. E., International Reference Geomagnetic Field: the seventh generation, *J. Geomagn. Geoelectr.*, *49*, 121–146, 1997.

Budden, K. G., *The Propagation of Radio Waves*, 667 pp., Cambridge Univ. Press, New York, 1988.

Jacobson, A. R., S. O. Knox, R. Franz, and D. C. Enemark, FORTE observations of lightning radio-frequency signatures: Capabilities and basic results, *Radio Sci.*, *34*(2), 337–354, 1999.

Massey, R. S., S. O. Knox, R. C. Franz, D. N. Holden, and C. T. Rhodes, Measurements of transionospheric radio propagation parameters using the FORTE satellite, *Radio Sci.*, *33*(6), 1739–1753, 1998.

A. R. Jacobson and X.-M. Shao, Space and Atmospheric Sciences Group, Mail Stop D466, Los Alamos National Laboratory, Los Alamos, NM 87545. (ajacobson@lanl.gov)

(Received September 8, 2000; revised January 8, 2001; accepted January 9, 2000.)